Experimental and theoretical investigations of strongly correlated $FeSb_{2-x}Sn_x$

A. Bentien, G. K. H. Madsen, S. Johnsen, and B. B. Iversen
Department of Chemistry, University of Aarhus, Langelandsgade 140, 8000 Aarhus C, Denmark
(Received 1 February 2006; revised manuscript received 11 August 2006; published 7 November 2006)

Thermopower, resistivity, and heat capacity have been measured on eight Sn-substituted $FeSb_{2-x}Sn_x$ samples with $x=0-0.15$. A giant peak in the low temperature thermopower of $FeSb_2$ is observed and is similar to what is found in the Kondo insulator FeSi. The *ab initio* calculated band structure of $FeSb_2$ shows striking similarities to that of FeSi. For the samples with Sn substitution the data indicate that as the Sn content increases $FeSb_{2-x}Sn_x$ evolves from a Kondo insulator into a heavy fermion metal similar to what is observed for $FeSi_{1-x}Al_x$.

DOI: 10.1103/PhysRevB.74.205105 PACS number(s): 72.20.−i, 75.50.Pp, 71.28.+d, 71.15.Mb

INTRODUCTION

In Kondo insulators and strongly correlated electron systems (SCES) with low charge carrier density (LCD), localized d or f states hybridize with conduction electron states leading to the formation of a small hybridization gap.[1] The density of states $[g(\varepsilon)]$ just below and above the hybridization gap becomes very large. The thermopower (S) is sensitive to variations in $g(\varepsilon)$ in the vicinity of the Fermi level (ε_F), and very large absolute values of S can be expected in Kondo insulators and SCES LCD. This is realized in number of compounds, e.g., FeSi,[2,3] $Ce_3Sb_4Pt_3$,[4–7] $CeFe_4P_{12}$,[1,8] $CeRu_4Sb_{12}$,[9] and CeB_6,[10] which all have pronounced peaks in $S(T)$ at low temperatures, where $|S|>100\ \mu V/K$.

Because of the large thermopower Kondo insulators and SCES LCD have the potential to become good thermoelectric materials for cooling applications at cryogenic temperatures. The cooling efficiency increases monotonically with the dimensionless figure of merit $ZT=S^2/(\rho\kappa)T$, where S is the thermopower, ρ is the electrical resistivity, κ is the thermal conductivity, and T is the temperature. Some of the listed compounds have enhanced power factors (S^2/ρ) that are comparable to or several times larger than observed for Bi_2Te_3,[11] which is the state-of-art thermoelectric material for cooling applications.

$FeSb_2$ (Fig. 1) is a well-studied compound[12–16] and the thermoelectric properties are known at room temperature and above for Te substituted samples ($FeSb_{2-x}Te_x$).[17–19] Our interest in this compound was initiated from band structure calculations, which showed a striking similarity to the electronic band structure of FeSi,[20–22] which is the prototypic example of a non-rare-earth containing Kondo insulator. Some of the properties measured below room temperature are the magnetic susceptibility (χ), the electrical resistivity,[23,24] and the Mössbauer effect.[25] In Ref. 24 the resistivity was found to be very anisotropic. $FeSb_2$ has been characterized as a highly correlated diamagnetic small band gap semiconductor[26] and in a recent publication as a Kondo insulator[27] with properties similar to FeSi. Furthermore, it is interesting to note a large temperature dependence of the quadrupole splitting with temperature,[25] also found in FeSi.[22]

The paper is organized as follows. First we present the calculated band structure, the measured transport properties (ρ and S) and heat capacities of eight $FeSb_{2-x}Sn_x$ samples with $x=0$, 0.01, 0.02, 0.03, 0.06, 0.09, 0.12, and 0.15. We then discuss the relevance of the Kondo insulator picture of the $x=0$ sample and the possibility that $FeSb_{2-x}Sn_x$ evolves into heavy Fermion metal as x increases. Preliminary results from our studies were published as a proceedings paper.[28] $S(T)$ for the $x=0$ sample has a large peak in $S(T)$ at low temperatures, similar to that of FeSi, supporting the Kondo insulator description of $FeSb_2$.

SAMPLE PREPARATION AND MEASUREMENT DETAILS

$FeSb_2$ can be synthesized by several methods.[12,17,18,23,24] In this study stoichiometric amounts of Fe, Sb, and Sn are rapidly heated to 1050 °C in evacuated quartz ampoules, kept at this temperature for 30 min, and subsequently quenched in water. This step leads to a variety of phases ($FeSb_2$, FeSb, Sb, and SbSn), but single phase $FeSb_2$ can be obtained by annealing at 600 °C in evacuated quartz ampoules for one week. It is observed that as the Sn content increases the samples become less brittle and more metal-

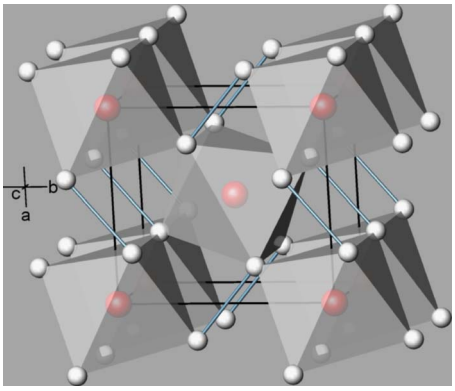

FIG. 1. (Color online) Structure of $FeSb_2$. Red (dark) atoms are Fe and white atoms are Sb. The unit cell is orthorhombic with $a=5.83$ Å, $b=6.54$ Å, and $c=3.20$ Å and the structure belongs to space group No. 58 (*Pnnm*). The Sb atoms are tetrahedrally coordinated by three Fe atoms and one Sb atom. The Fe atoms are octahedrally coordinated by six Sb atoms. The Fe-Sb and Sb-Sb dimer (dark, blue) bonds are 2.58 Å, 2.60 Å, and 2.88 Å, respectively. There are no direct Fe-Fe bonds and the shortest Fe-Fe distance is 3.20 Å. The unit cell contains two formula units.

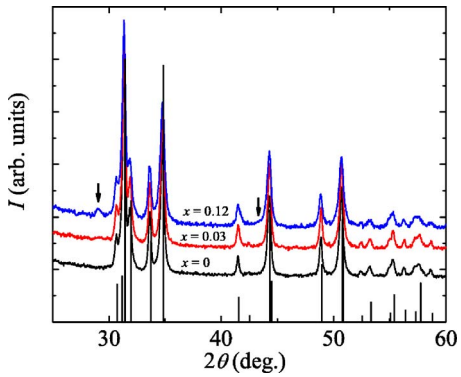

FIG. 2. (Color online) X-ray powder diffraction patterns of $FeSb_{2-x}Sn_x$ with $x=0$ (black), 0.03 (red), and 0.12 (blue). Vertical bars indicate the position and magnitude of the theoretical peaks for $FeSb_2$. Arrows indicate the position of the two strongest diffraction peaks of the SbSn alloy.

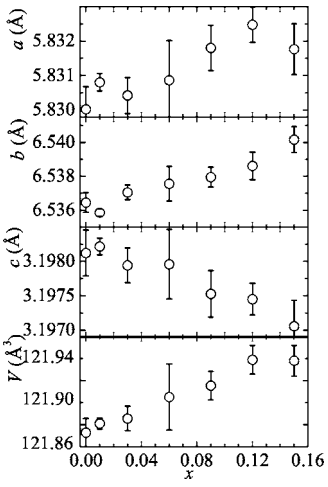

FIG. 3. Lattice parameters and unit cell volume for $FeSb_{2-x}Sn_x$ as function of x (the nominal stoichiometry).

like. Densities measured on large samples are about 94% of the theoretical density. For all samples x-ray powder diffraction patterns were recorded on a STOE diffractometer equipped with a position sensitive detector and using Cu Kα1 radiation obtained from a germanium monochromator. As examples, Fig. 2 shows representative x-ray diffraction patterns of the $x=0$, 0.03, and 0.12 samples. All diffraction patterns are consistent with $FeSb_{2-x}Sn_x$ having the $FeSb_2$ structure. All Sn containing samples had small traces of SbSn, but with much less concentration than the nominal Sn concentration. Besides this all samples contain a magnetic impurity, probably Fe_3O_4 which orders ferrimagnetically at 853 K with an average saturation moment of $1.27\mu_B$ per Fe.[29] From the magnetization as function of the magnetic field (data not shown) the Fe_3O_4 content can be estimated to be of the order one Fe_3O_4 per 300 $FeSb_2$, except for the $x=0.02$ sample where it is several times larger. The $x=0.02$ sample is subsequently left out of the analysis. Figure 1 summarizes some of the structural features of $FeSb_2$. The lattice parameters of all samples were determined at 22 °C on a D8 Bruker powder diffractometer with monochromatic Cu Kα1 radiation using LaB_6 as an internal standard (a_{LaB6} =4.15692 Å). The results can be seen in Fig. 3. The a and b axes have a clear increase as a function of the nominal Sn content (x), whereas the c axis decreases with increasing x. Since the covalent radius for Sn (1.41 Å) is slightly larger than for Sb (1.38 Å) an increase of all three lattice parameters would be expected. In the c direction there are only Fe-Sb bonds, and the data therefore indicate that Fe-Sb/Sn bonds are strengthened as Sb is substituted with Sn. In $FeSb_{2-x}Te_x$ the reverse effect is observed, the a and b axes decrease whereas the c axis increases with increasing Te content.[17]

Transport properties and specific heat (C_p) were measured on a Quantum Design physical properties measurement system (PPMS). For the transport measurements a four point contact technique was used. The samples were cut from the annealed bulk material, and visible cracks were avoided. Typical sample dimensions were 5 mm×5 mm×14 mm. For the specific heat measurements, samples with masses 20–25 mg were used. They were cut from vicinity of the samples used for the transport measurements. For the specific heat measurements a new calibration of the sample holder thermometers was made. C_p of the sample holder and contact grease were measured prior to mounting the sample. C_p of the grease did not contribute more than 3% of the C_p of the sample and the sample always contributed more than 60% of the total C_p at any temperature. For measurements at $T<310$ K samples were mounted with N grease and for $T>290$ K H grease was used. Data in the overlapping region were the same within errors and data sets were merged without any scaling.

BAND STRUCTURE

The calculations were performed using the L/APW+lo method as implemented in the WIEN2k code.[30] A plane wave cutoff defined by $\min(R\alpha)\max(k_n)=5.5$ and sphere sizes of 2.5 a_0 (Fe) and 2.2 a_0 (Sb) were used. Spin-orbit coupling was included and an energy cutoff of 2.4 Ry for the second variational basis set was used. 330 k points on a shifted mesh in the irreducible Brillouin zone were used for the self-consistent calculations.

The electronic structure of the marcasite compounds was analyzed qualitatively by Goodenough[31] and valence states can be expected to be dominated by the Fe 3d states and the Sb 5sp states. Figure 4 shows the calculated $g(\varepsilon)$ and it is seen that $g(\varepsilon_F)$ is small but has a nonzero value slightly larger than 1 states per eV per unit cell [states/(eV u.c.)]. This is due to a maximum of the highest valence band at the $\pi(111)$ point and a minimum of the lowest conduction band along the Γ-$\pi(111)$ line (not shown). The direct gap is calculated to be around 0.2 eV.

The Fe atoms are located on sites with C_{2h} $(2/m)$ symmetry. In Table I the integrated populations of the Fe d states in a local coordinate system corresponding to the symmetry direction with z parallel to the two fold axes are given. The d_{z^2} orbital is destabilized and the Fermi level is found between peaks with mainly d_{z^2} and $d_{x^2-y^2}$ character but other-

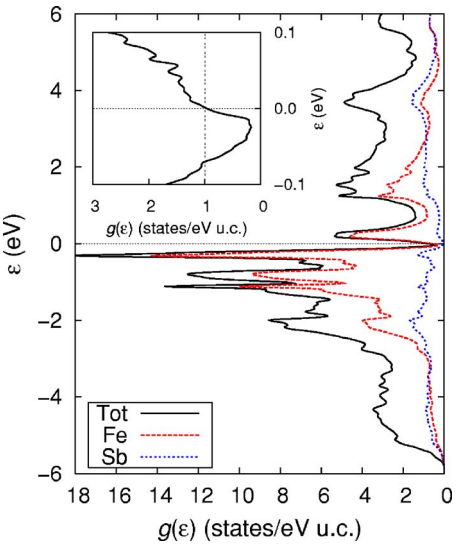

FIG. 4. (Color online) The main panel shows the density of states (g) of $FeSb_2$ as a function of electron energy (ε). The straight dotted line represents the Fermi level (ε_F). Inset is a replot of the same data in the vicinity of the Fermi level, a nonzero $g(\varepsilon_F)$ is observed. The unit cell contain two $FeSb_2$ formula units.

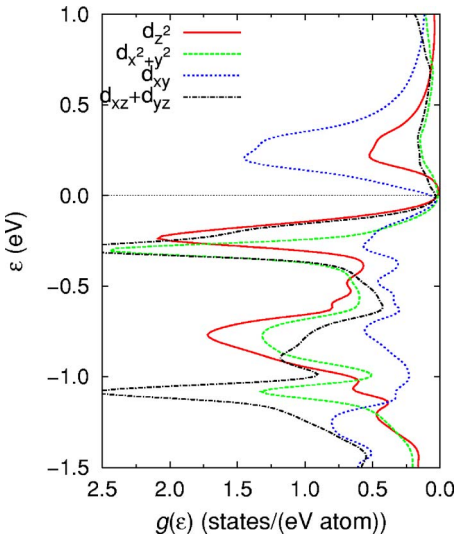

FIG. 5. (Color online) Projected density of states with respect to a coordinate system with the z axis parallel to the short Fe-Sb bond and the x axis parallel to the long Fe-Sb bond (the "chemical axes" in Table I). The straight dotted line represents the Fermi level.

wise the orbital populations do not form a clear pattern. One can choose a local coordinate system with the z axis along the short axial Fe-Sb bond (2.58 Å) and the x and y axes along the longer Fe-Sb bonds (2.60 Å). These axes do not correspond to symmetry operators, but reflect the slightly distorted octahedral environment with a small tetragonal ($\bar{4}2m/D_{2d}$) splitting. Using these "chemical axes" the orbital populations form a clear pattern, Table I and Fig. 5. The orbitals directed towards the ligands, d_{z^2} and $d_{x^2-y^2}$, which are usually destabilized in an ionic crystal field, are stabilized. The stabilization of d_{z^2} and $d_{x^2-y^2}$ agree with a covalent bonding scheme as would be expected from the formation of a hybridization gap, necessary for the formation of a Kondo insulator. Furthermore it is seen that the least populated orbital, d_{xy}, lies in the plane with the weakest Fe-Sb bonds, again reflecting a mainly covalent bonding scheme.

RESISTIVITY AND THERMOPOWER

Figure 6 shows $\rho(T)$ for all samples in the temperature range from 2 K to 400 K. All samples have negative temperature coefficients in the entire temperature range. For the $x=0$ sample ρ decreases almost three orders of magnitude from 2 K to 400 K, and the magnitude and temperature dependence is similar to that observed for other polycrystalline samples in the literature.[17,19] When compared to $\rho(T)$ of single crystalline $FeSb_2$ samples[23,24] there are notable differences. In Ref. 24 $\rho(T)$ along the b axis is found to be metallike with increasing ρ for temperatures above approximately 25 K. $\rho(T)$ along the a and c axis was observed to have semiconducting temperature dependencies in the whole temperature range[24] and similar to what is observed in Ref. 23. A direct comparison of our data with the ones of Ref. 24 is difficult since $\rho(T)$ data along the a and c axis in the temperature range from 10 K to 70 K are only plotted as ln ρ vs T^{-1} in small insets. At room temperature ρ of our sample is about ten times larger than that of the samples in Refs. 23 and 24. If it is assumed that ρ of a polycrystalline sample can be found from the average of the three axes, the temperature dependence is very similar down to at least 70 K. At lowest temperatures ρ is of the same order of magnitude but with different temperature dependencies. Together this indicates that the larger ρ in our $FeSb_2$ sample at room temperature is due to grain boundary scattering and that impurity states

TABLE I. Orbital occupations calculated in two different axes systems.

	d_{z^2}	$d_{x^2-y^2}$	d_{xy}	d_{xz}	d_{yz}
Symmetry axes	0.99	1.40	1.27	1.36	1.50
"Chemical" axes	1.41	1.44	1.09	1.25	1.31

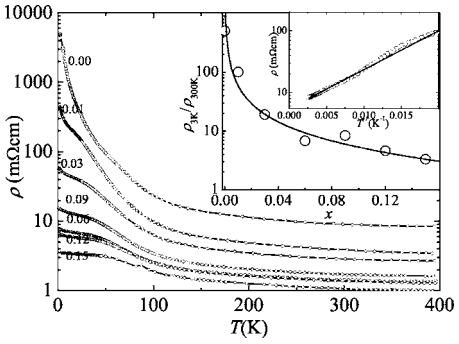

FIG. 6. Resistivity (ρ) as function of temperature (T) for the $FeSb_{2-x}Sn_x$ samples. Inset shows ρ_{3K}/ρ_{300K} as a function of x. The solid line is a guide to the eye. The second inset is an Arrhenius plot of $\rho(T)$ for the $x=0$ sample. The solid line is a linear fit to data above 50 K with an activation energy of 265 K.

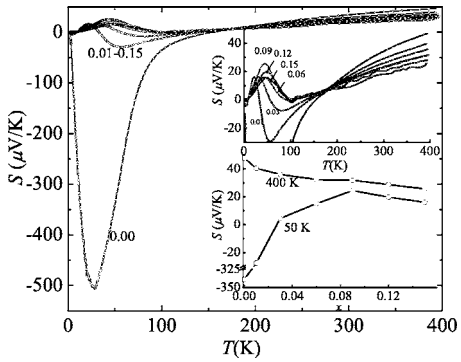

FIG. 7. Thermopower (S) as function of temperature (T) for the $FeSb_{2-x}Sn_x$ samples. Upper inset is a replot of the same data with a much reduced y scale. Lower inset shows S as a function of x at 50 K and 200 K (note the broken y axis).

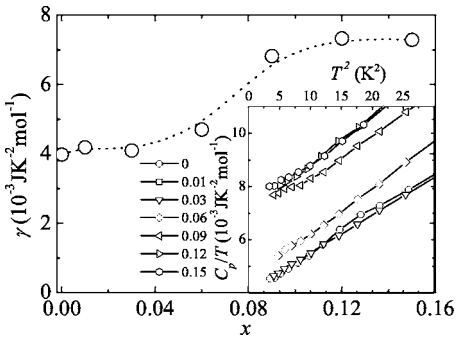

FIG. 8. Sommerfeld coefficient (γ) of $FeSb_{2-x}Sn_x$ as a function of x. Dotted curve is a guide to the eye. Inset shows the specific heat divided by temperature (C_p/T) as a function of T^2 at lowest temperatures. Linear fits (not shown) to the curves are used to extract γ with the relation $C_p/T=\gamma+\beta T^2$.

have a larger influence at lowest temperatures than in Ref. 24. The inset of Fig. 6 shows ρ_{3K}/ρ_{300K} as function of Sn content. The decrease of ρ_{3K}/ρ_{300K} with increasing Sn content indicates an increasing metallic behavior, as expected if the charge carrier concentration increases. Arrhenius plots of the $\rho(T)$ data above 50 K shows that the activation energy is approximately 265 K for the pure sample, see inset of Fig. 6. This is close to an average of the three axes from Ref. 24. The activation energy has a tendency to decrease with increasing Sn content.

Figure 7 shows $S(T)$ for all samples in the temperature range from 2 K to 400 K. For the $x=0$ sample S decreases rapidly with increasing temperature and reaches a minimum of approximately -500 μV/K at 25 K. As the temperature increases further S increases and becomes positive around 150 K. S continues to increase monotonically to a value of almost 50 μV/K at 400 K. The room-temperature value of the thermopower is $S=34$ μV/K, which is in good agreement with other polycrystalline samples in the literature where $S\sim 31$ μV/K has been reported.[18,19]

For the samples with $x>0$ the temperature dependence and magnitude of S is different. The upper inset shows the same data as Fig. 7, but on a reduced ordinate scale. It is seen that S increases to a value of 15–25 μV/K around 25 K to 50 K, depending on the Sn content. This is followed by a decrease, where S becomes negative for the samples with the lowest Sn content ($x=0.01, 0.03$). Above 150 K S increases with temperature, similarly to the undoped sample, although the magnitude of S is slightly reduced. The lower inset of Fig. 7 shows the dependence of S on the Sn content measured at 50 K and 400 K, which are the temperatures at which S shows the largest variation among samples with $x>0$ (50 K) and the maximum measurement temperature (400 K). S has a monotonic dependence on x. Initially S increases with x up to $x=0.09$ followed by a small decrease. Above 200 K S is positive for all samples and increases monotonically with temperature, but the increase becomes smaller with temperature. As the Sn content increases S becomes lower. Qualitatively such behavior can be explained by the Mott formula $S=\pi^2 k_B^2 T/(3e)[\partial \ln \sigma/\partial\varepsilon]_{\varepsilon=\varepsilon_F}$, where e is the electron charge.[32] In a one parabolic band approximation the Mott formula states that S increases linearly with temperature and decreases with increasing charge carrier concentration. In Ref. 23 measurements show that the Hall coefficient of $FeSb_2$ decreases with increasing temperature. In a one band model this can be interpreted as if the concentration of charge carriers increases with temperature and this explain why S increases less than linearly with temperature. Substitution of Sb with Sn corresponds to the creation of a hole. The hole concentration increases with increasing Sn and this can explain the decrease of S with increasing x above 200 K.

In the Kondo insulator FeSi a giant peak in $S(T)$ with very similar temperature dependence is also observed, but at 50 K and with a positive value of 500 μV/K.[2,33] The theoretical investigations of the thermopower of FeSi are scarce in the literature.[34,35] Besides both the magnitude and temperature dependence of the theoretical $S(T)$ are similar to what is observed for $FeSb_2$, theoretical investigations also predict that $S(T)$ is sensitive to small changes in the charge carrier concentration/doping, as also observed experimentally.[2,3,36] For the $FeSb_{2-x}Sn_x$ samples the large peak in $S(T)$ at 25 K is suppressed, even for the $x=0.01$ sample. For normal valence semiconductors such a strong sensitivity of S on the doping is not expected, however, for strongly correlated electron systems this is not unusual. $S(T)$ for samples with $x>0$ is similar to what is observed for heavy fermion compounds where $S(T)$ can change between positive and negative values at lowest temperatures.[37]

The thermoelectric properties of $FeSb_{2-x}Sn_x$ are modest. For the $x=0$ sample at 25 K ρ and S are 315 mΩ cm and -500 μV/K, respectively. This leads to a power factor $S^2/\rho=0.8\times10^{-4}$ W m^{-1} K^{-2}, a factor of 10–100 times lower than observed for the best thermoelectric materials. Combining the power factor with the thermal conductivity[28] leads to a ZT value of $\sim$0.001 at 25 K. For samples with $x>0$ the thermoelectric figures of merit values are even lower.

SPECIFIC HEAT

Low temperature $C_p(T)$ was measured on all samples and the results at low temperature can be seen in the inset of Fig. 8, where $C_p(T)/T$ is plotted as function of T^2. The relation

$C_p/T=\gamma+\beta T^2$ has been fitted to all data sets in the temperature range from 1.8 K to 6 K. The Sommerfeld coefficient γ represents the electronic contribution and the βT^2 term the phononic contribution with $\beta=12\pi NR/(5\theta_D^3)$. N and R are the concentration of atoms and the gas constant, respectively. From β, Debye temperatures of $\theta_D \approx 330-350$ K are found for all samples, in relatively good agreement with 380 K obtained from Mössbauer spectroscopy.[25] In Ref. 27 θ_D is reported to be 256 K, however, $C_p/T(T^2)$ has a tendency to increase faster than T^2 and fits that include data at higher temperatures will lead to a lower θ_D. The main panel of Fig. 8 shows a clear increase of γ with increasing x.

The $x=0$ sample has a nonzero residual γ value of 3.98×10^{-3} J K^{-2} mol^{-1}. With the free electron expression $\gamma=\pi^2 k_B^2 g(\varepsilon_F)/3$, $g(\varepsilon_F)$ for the $x=0$ sample can be calculated to be 3.4 states/(eV u.c.). As mentioned earlier a residual electronic contribution is in fact also predicted from the band structure calculations. This can be seen from the inset of Fig. 4 where $g(\varepsilon_F)$ is predicted to be slightly larger than 1.0 states/(eV u.c.), which is somewhat smaller than estimated from experiment. Further experiments on more pure single crystalline samples must be conducted to make any definite conclusion about the electronic states at the Fermi level. For FeSi γ has been reported to range from 0.63×10^{-3} J K^{-2} mol^{-1} to 2.2×10^{-3} J K^{-2} mol^{-1}.[38–40] For the other $FeSb_{2-x}Sn_x$ samples γ corresponds to $g(\varepsilon_F)$ ranging from 3.5 states/(eV u.c.) to 6.2 states/(eV u.c.) in a free electron model.

For the samples with $x>0$ an estimate of the charge carrier mass (m^*) can be calculated from the Sommerfeld coefficient and free electron model expression $g(\varepsilon_F)=m^* k_F/(\hbar^2\pi^2)$, where the Fermi wave number $k_F=(3\pi^2 n)^{1/3}$. Assuming that the charge carrier density (n) equals x holes per $FeSb_{2-x}Sn_x$, m^* is in the range from 10 m_e to 15 m_e for all samples. The specific heat data combined with the thermopower and resistivity data indicate that $FeSb_{2-x}Sn_x$ evolves from a strongly correlated semiconductor into a metallic moderately heavy fermion system as x becomes larger than 0.15. With respect to $\rho(T)$ and the low temperature $C_p(T)$ of $FeSb_{2-x}Sn_x$ it is very similar to $FeSi_{1-x}Al_x$, which is an example of system that evolves from a strongly correlated semiconductor to a heavy fermion system as the Al content increases.[41]

Figure 9 shows $C_p(T)$ from 1.8 K to 350 K for the $x=0$ and 0.15 sample and the inset shows the same data plotted in the high temperature region. At 300 K C_p for the $x=0$ sample is 3.5 J K^{-1} mol^{-1} (4%) larger than for the $FeSb_2$ samples in Ref. 27. At lowest temperatures a comparison is not possible because reliable data below 50 K cannot be extracted from Fig. 6 in Ref. 27. Since no secondary phases, other than a tiny amount of Fe_3O_4, are present this discrepancy is difficult to explain. The dashed curve in the inset of Fig. 9 is the theoretical expectation from the two band model of Ref. 27 combined with a Debye model. It is seen that the measured $C_p(T)$ is tracked quite well from 150 K up to 350 K. For the $x=0.15$ sample $C_p(T)$ is slightly larger than that of the $x=0$ sample as expected if the charge carrier concentration is larger in the former. However, above 100 K $C_p(T)$ of the $x=0.15$ sample starts to become lower than that of the $x=0$ sample. We attribute this to differences in the electronic contribution and we explain it by the $x=0.15$ being almost metallic, because the Fermi level has been shifted away from the band gap to lower values compared to the $x=0$ sample. In this case the specific heat due excitation across the band gap diminishes whereas a normal linear with T electronic term starts to emerge. This interpretation is supported by a theoretical study of the band structure of $FeSi_{1-x}Al_x$ which shows that the Al substitution to a good approximation can be described by a rigid band where the Fermi level is shifted to lower values as the Al content increases.[34] Because of the similarities between $FeSb_{2-x}Sn_x$ and $FeSi_{1-x}Al_x$,[41,42] we believe this also to be the case for $FeSb_{2-x}Sn_x$.

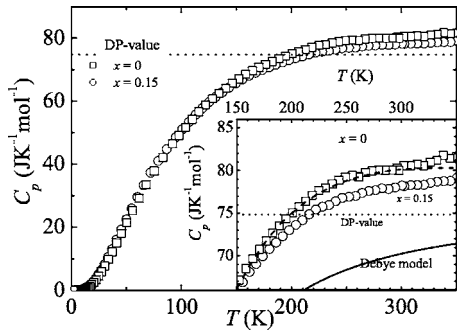

FIG. 9. Specific heat (C_p) per mole $FeSb_{2-x}Sn_x$ as function of temperature (T) for $x=0$ and $x=0.15$. The dotted line is the classical Dulong Petit value $3NR=74.8$ J K^{-1} mol^{-1}. Inset shows the same data in the high temperature region. The solid curve is a Debye model calculation with three atoms per unit cell and a Debye temperature of 340 K. The dashed curve is a sum between the Debye model and the contribution from two narrow bands where the total density per band is 2.96 states per unit cell (1.48 per formula unit), the band gap is 862 K, and the band width is 295 K, see Ref. 27.

CONCLUSIONS

We have presented transport and thermodynamic properties of eight Sn-substituted $FeSb_{2-x}Sn_x$ samples in combination with a $FeSb_2$ band structure calculation. The undoped $FeSb_2$ has a giant peak in $S(T)$ of -500 μV/K at 25 K. A similar peak is observed for FeSi,[2,33] and this type of behavior is in agreement with theoretical predictions for Kondo insulators.[35,43]

$C_p(T)$ for the $x=0$ sample clearly shows excess contributions to C_p above 150 K, as also observed for FeSi. Use of a simple two narrow band model and a Debye model describes $C_p(T)$ reasonably well. The high temperature $C_p(T)$ of the $x=0.15$ sample can be described quite well with a Debye model and a linear in T contribution as expected for a metallic system. The Sommerfeld coefficient increases with Sn content and the effective mass of the charge carriers can be estimated to be in the range 10–15 m_e. Together with the magnitude and temperature dependence of $\rho(T)$ and $S(T)$ this indicates that $FeSb_{2-x}Sn_x$ evolves from a strongly correlated semiconductor for $x=0$, into a moderately heavy fermion

system for samples with $x > 0.15$, being similar to what is observed for $FeSi_{1-x}Al_x$ with increasing Al substitution.

ACKNOWLEDGMENTS

The Danish Research Council for Technology and Production is thanked for funding this work. We are indebted to the Carlsberg Foundation and the Danish Research Councils for a Quantum Design PPMS. G.K.H.M. thanks the Carlsberg Foundation for financial support. The Danish Center of Scientific Computing is thanked for allocated computer time.

[1] G. Aeppli and Z. Fisk, Comments Condens. Matter Phys. **16**, 155 (1992).
[2] R. Wolfe, J. H. Wernick, and S. E. Hazko, Phys. Lett. **19**, 449 (1965).
[3] B. C. Sales, E. C. Jones, B. C. Chakoumakos, J. A. Fernandez-Baca, H. E. Harmon, J. W. Sharp, and E. H. Volckmann, Phys. Rev. B **50**, 8207 (1994).
[4] M. Kasaya, K. Katoh, and K. Takegahara, Solid State Commun. **78**, 797 (1991).
[5] K. Katoh, and M. Kasaya, J. Phys. Soc. Jpn. **65**, 3654 (1996).
[6] C. D. W. Jones, K. A. Regan, and F. J. DiSalvo, Phys. Rev. B **60**, 5282 (1999).
[7] C. D. W. Jones, K. A. Regan, and F. J. DiSalvo, Phys. Rev. B **58**, 16057 (1998).
[8] H. Sato, Y. Abe, H. Okada, T. D. Matsuda, K. Abe, H. Sugawara, and Y. Aoki, Phys. Rev. B **62**, 15125 (2000).
[9] K. Abe, H. Sato, T. D. Matsuda, T. Namiki, H. Sugawara, and Y. Aoki, J. Phys.: Condens. Matter **14**, 11757 (2002).
[10] S. R. Harutyunyan, V. H. Vardanyan, A. S. Kuzanyan, V. R. Nikoghosyan, S. Kunii, K. S. Wood, and A. M. Gulian, Appl. Phys. Lett. **83**, 2142 (2003).
[11] G. D. Mahan, in *Solid State Physics*, Vol. 51 (1998), p. 81.
[12] H. Holseth and A. Kjekshus, J. Less-Common Met. **16**, 472 (1968).
[13] H. Holseth and A. Kjekshus, Acta Chem. Scand. (1947-1973) **22**, 3273 (1968).
[14] H. Holseth and A. Kjekshus, Acta Chem. Scand. (1947-1973) **22**, 3284 (1968).
[15] H. Holseth and A. Kjekshus, Acta Chem. Scand. (1947-1973) **23**, 3043 (1969).
[16] H. Holseth, A. Kjekshus, and A. F. Andresen, Acta Chem. Scand. (1947-1973) **24**, 3309 (1970).
[17] G. Yamaguchi, M. Shimada, M. Koizumi, and F. Kanamaru, J. Solid State Chem. **34**, 241 (1980).
[18] N. K. Abrikosov and L. I. Petrova, Inorg. Mater. **25**, 1087 (1989).
[19] L. I. Petrova, N. K. Abrikosov, L. D. Dudkin, V. M. Sokolova, and V. V. Musaelyan, Inorg. Mater. **26**, 1023 (1990).
[20] L. F. Mattheiss and D. R. Hamann, Phys. Rev. B **47**, 13114 (1993).
[21] C. Fu, M. P. C. M. Krijn, and S. Doniach, Phys. Rev. B **49**, 2219 (1994).
[22] N. E. Christensen, I. Wenneker, A. Svane, and M. Fanciulli, Phys. Status Solidi B **198**, 23 (1996).
[23] A. K. L. Fan, G. H. Rosentha, H. L. McKinzie, and A. Wold, J. Solid State Chem. **5**, 136 (1972).
[24] C. Petrovic, J. W. Kim, S. L. Bud'ko, A. I. Goldman, P. C. Canfield, W. Choe, and G. J. Miller, Phys. Rev. B **67**, 155205 (2003).
[25] J. Steger and E. Kostiner, J. Solid State Chem. **5**, 131 (1972).
[26] C. E. T. Goncalves da Silva, Solid State Commun. **33**, 63 (1980).
[27] C. Petrovic, Y. Lee, T. Vogt, N. Dj. Lazarov, S. L. Bud'ko, and P. C. Canfield, Phys. Rev. B **72**, 045103 (2005).
[28] A. Bentien, G. K. H. Madsen, S. Johnsen, and B. B. Iversen, in *Proceedings of the 24th International Conference on Thermoelectrics* (IEEE, Piscataway, NJ, 2005).
[29] E. Du Trémolet de Lacheisserie, D. Gignoux, and M. Schlenker, *Magnetism II—Materials and Applications* (Kluwer, Norwell, MA, 2002).
[30] P. Blaha, K. Schwarz, G. K. H. Madsen, D. Kvasnicka, and J. Luitz, *WIEN2k, An Augmented Plane Wave Plus Local Orbitals Program for Calculating Crystal Properties* (Vienna University of Technology, Vienna, Austria, 2001).
[31] J. B. Goodenough, J. Solid State Chem. **5**, 144 (1972).
[32] F. J. Blatt, P. A. Schroeder, C. L. Foiles, and D. Greig, *Thermoelectric Power of Metals* (Plenum Press, New York, 1976).
[33] B. C. Sales, E. C. Jones, B. C. Chakoumakos, J. A. Fernandez-Baca, H. E. Harmon, J. W. Sharp, and E. H. Volckmann, Phys. Rev. B **50**, 8207 (1994).
[34] T. Jarlborg, Phys. Rev. B **59**, 15002 (1999).
[35] T. Saso and K. Urasaki, J. Phys. Chem. Solids **63**, 1475 (2002).
[36] B. Buschinger, C. Geibel, F. Steglich, D. Mandrus, D. Young, J. L. Sarrao, and Z. Fisk, Physica B **230–232**, 784 (1997).
[37] E. Bauer, Adv. Phys. **400**, 417 (1991).
[38] V. Jaccarino, G. K. Wertheim, J. H. Wernick, L. R. Walker, and S. Arajs, Phys. Rev. **160**, 476 (1967).
[39] M. A. Chernikov, L. Degiorgi, E. Felder, S. Paschen, A. D. Bianchi, H. R. Ott, J. L. Sarrao, Z. Fisk, and D. Mandrus, Phys. Rev. B **56**, 1366 (1997).
[40] S. Paschen, E. Felder, M. A. Chernikov, L. Degiorgi, H. Schwer, H. R. Ott, D. P. Young, J. L. Sarrao, and Z. Fisk, Phys. Rev. B **56**, 12916 (1997).
[41] J. F. DiTusa, K. Friemelt, E. Bucher, G. Aeppli, and A. P. Ramirez, Phys. Rev. Lett. **78**, 2831 (1997).
[42] J. F. DiTusa, K. Friemelt, E. Bucher, G. Aeppli, and A. P. Ramirez, Phys. Rev. B **58**, 10288 (1998).
[43] C. Grenzebach and G. Czycholl, Physica B **359**, 732 (2005).